ECS Journal of Solid State
Science and Technology

OPEN ACCESS

Cathodoluminescence and Photoluminescence of $YPO_4:Pr^{3+}$, $Y_2SiO_5:Pr^{3+}$, $YBO_3:Pr^{3+}$, and $YPO_4:Bi^{3+}$

To cite this article: M. Broxtermann *et al* 2017 *ECS J. Solid State Sci. Technol.* **6** R47

Cathodoluminescence and Photoluminescence of $YPO_4:Pr^{3+}$, $Y_2SiO_5:Pr^{3+}$, $YBO_3:Pr^{3+}$, and $YPO_4:Bi^{3+}$

M. Broxtermann,[a] D. den Engelsen,[b] G. R. Fern,[b] P. Harris,[b] T. G. Ireland,[b,z] T. Jüstel,[a] and J. Silver[b]

[a]*Research Group Tailored Optical Materials, University of Applied Sciences Münster, D-48565 Steinfurt, Germany*
[b]*Centre for Phosphor and Display Materials, Wolfson Centre for Materials Processing, Brunel University London, Uxbridge, Middlesex UB8 3PH, United Kingdom*

Herein we describe the synthesis, characterization, and cathodoluminescence of the UV emitting phosphors $YPO_4:Pr^{3+}$, $Y_2SiO_5:Pr^{3+}$, $YBO_3:Pr^{3+}$, and $YPO_4:Bi^{3+}$. These photoluminescent UV phosphors exhibited strong luminescence in the UV part of the electromagnetic spectrum when excited by electron bombardment. Spectra have been recorded between 210 and 650 nm at electron beam energies of 5, 10 and 15 keV. The energy efficiencies of $YPO_4:Pr^{3+}$, $Y_2SiO_5:Pr^{3+}$, $YBO_3:Pr^{3+}$ and $YPO_4:Bi^{3+}$ in the UV range were 9.2%, 2.7%, 5.1%, and 7.2%, respectively at 15 keV. UV photoluminescence measurements were conducted using 160 nm excitation generated by combining a VUV monochromator with a deuterium lamp.
 [DOI: 10.1149/2.0051704jss]

Manuscript submitted November 21, 2016; revised manuscript received January 11, 2017. Published January 27, 2017.

The UV emitting phosphor $Y_2SiO_5:Pr^{3+}$ has attracted attention both because of its potential application as a UV tunable laser and also as a scintillator arising from its short decay time (of about 40 ns).[1–4] Moreover, it is one of the first UV emitting materials, which manifests up-conversion of blue radiation into the UV-C range.[5]

Interest rose in UV-A and UV-B emitting luminescent materials after the introduction of low-pressure Hg discharge lamps that were developed as sun tan lamps in the middle of the 20th century.[6] The early UV emitting phosphors were activated by Tl^+, Pb^{2+}, or Bi^{3+}, while later Ce^{3+} activated phosphors such as $LaPO_4$:Ce and YPO_4:Ce came into play due to their better stability and environmental compliance as they contained no hazardous elements.

The development of phosphors emitting in the UV-C range was stimulated by the advent of efficient dielectric barrier Xe discharge lamps some decades ago.[7–9] At that time, some UV-C emitting luminescent materials activated by Pr^{3+}, Nd^{3+}, Bi^{3+}, Pb^{2+}, or Tl^+ were already in focus. However, phosphors activated by Tl^+ or Pb^{2+} have since become less interesting due to the toxic character of these materials.

One of the most efficient UV-C emitting materials, which also has a rather high thermal quenching temperature, is YPO_4:Bi .[10] However a serious drawback with this material is the limited stability of Bi^{3+} cations toward oxidation or reduction. This necessitated a search for efficient and long-term stable Pr^{3+} activated materials, since it is thought that Pr^{3+} can withstand the harsh conditions of VUV radiation and the electron bombardment inside an excimer discharge tube. The most efficient materials amongst the many, which have been published so far are YPO_4:Pr, $LaPO_4$:Pr, Y_2SiO_5:Pr, YBO_3:Pr, $Ca_9Y(PO_4)_7$:Pr, $LuBO_3$:Pr, Lu_2SiO_5:Pr and $LuPO_4$:Pr. The later Lutetium containing compounds are also regarded as scintillators because of their high density.

Xe excimer discharge lamps containing a UV-C phosphor for germicidal action and photochemical purposes have been developed by several groups[11–13] and lamp products containing YPO_4:Nd, YPO_4:Pr, YPO_4:Bi, and $LaPO_4$:Pr were introduced several years ago. Even though these lamps can achieve wall plug efficiency close to that of low- and medium-pressure Hg discharge lamps, their commercial success is rather moderate so far. The main reason for this observation is their lower long-term stability, which is a very important consideration for any industry marketing the application of UV radiation.

Due to the fact that the fluorescent Xe excimer discharge lamps have some serious stability problems, we decided to investigate the spectra and efficiency of these materials under CL excitation. A theoretical estimation of the efficiency, $\eta_{CL,}$ of a UV-C emitting CL phosphor is possible by using the equation $\eta_{CL} = S{\cdot}E_{h\nu}/\varepsilon{\cdot}E_g$, where S = the transfer probability, $E_{h\nu}$ = the energy of emitted photons and ε = a dimensionless number that expresses the creation energy of an electron-hole pair in terms of E_g, which is the bandgap of the CL phosphor host.[14] This simple approach shows that a 5 eV photon emitting phosphor with a bandgap of 8.0 eV could achieve an η_{CL} of 21%, if ε is 2.0 and S = 0.66. This is close to the value of the ZnS based phosphors used in cathode ray tubes.[14] The qualitative recording of CL spectra is straightforward as long as the excitation is below the saturation limit of the phosphor. Quantitative measurement of the energy efficiency of CL is more complicated, because secondary electron emission and charging of the phosphor powder makes the determination of the primary E-beam current that is hitting the phosphor less straightforward. Recently we have described a measuring method for determining the CL efficacy and energy efficiency of phosphor powders in the case of charging.[15,16] We have slightly modified this method for determining the energy efficiency of the above mentioned UV phosphors.

Experimental

Materials and synthesis pathways.—*YPO_4:Bi.*—Y_2O_3 (Treibacher, 99.99%) and Bi_2O_3 (Merck, p.a.) were dissolved in concentrated boiling HNO_3 (Bernd Kraft, 65%). The amount of Bi_2O_3 was adjusted in order to reach a final dopant concentration of 0.7% as substituent for yttrium within the YPO_4 host. The translucent solution was then diluted with deionized water. The resulting solution was allowed to cool down to room-temperature before it was added dropwise to a saturated aqueous solution of oxalic acid (Merck, synthesis quality). The precipitated material was filtered off and repeatedly washed with deionized water and ethanol before it was dried and calcined at 1000°C for 5 hours. The thus synthesized oxalate-precursor was then mixed with ammonium hydrogen phosphate (Sigma Aldrich, ACS grade) and 1 wt.-% LiF (Alfa Aesar, 99.89%) and thoroughly blended under addition of acetone. The dried mixture was then annealed under regular atmosphere at 1000°C for 6 hours. This resulted in a partially sintered material that was coarsely crushed in a mortar and pestle before it was wet-milled to an average particle size of about 6 µm using a roller belt. The final white powder was then stirred in water for about 30 minutes before it was filtered off and dried at 80°C for several hours.

YPO_4:Pr.—Y_2O_3 and Pr_6O_{11} (Treibacher, 99.99%) were dissolved in concentrated boiling HNO_3 with an amount of Pr_6O_{11} yielding a 1% substitution of yttrium by praseodymium in the final product. The translucent solution was then diluted with deionized water. The

[z]E-mail: Terry.ireland@brunel.ac.uk

resulting solution was allowed to cool down to room-temperature before it was dropwise added to a cold-saturated aqueous solution of oxalic acid. The precipitated material was filtered off and repeatedly washed with deionized water and ethanol before it was dried and calcined at 1000°C for 2 hours. The thereby synthesized oxalate-precursor was then mixed with ammonium hydrogen phosphate and 1 wt.-% LiF and thoroughly mixed under addition of acetone. The dried mixture was then annealed under regular atmosphere at 1000°C for 6 hours followed by another annealing step under a reducing CO atmosphere at 1000°C for 6 hours. This resulted in a partially sintered material which was then coarsely crushed in a mortar and pestle before it was wet-milled to an average particle size of about 6 μm using a roller belt. The final white powder was then stirred in water for about 30 minutes before it was filtered off and dried at 80°C for several hours.

YBO_3:Pr.—Y_2O_3 was mixed with 2 mol-% excess H_3BO_3 (Merck, ACS grade) and Pr_6O_{11} so that the final product contained 1% praseodymium as substituent for yttrium. The mixture was thoroughly crushed in an agate mortar under the addition of acetone. The mixture was then dried at 80°C before the first calcination step for 2 hours in a regular atmosphere at 800°C followed by a further calcination for 12 hours at 1200°C under a reducing CO atmosphere. This resulted in a partially sintered material that was dry-milled in an agate mortar and pestle to a mean particle size of about 5 μm. The final white and greenish tinted powder was then stirred in water for about 30 minutes before it was filtered off and dried at 80°C for several hours.

Y_2SiO_5:Pr.—Y_2O_3, Pr_6O_{11} and SiO_2 were weighted in order to reach a final stoichiometry of $Y_{1.98}SiO_5$:$Pr_{0.02}$ and completely dissolved in concentrated HNO_3. The diluted clear solution was then added dropwise into a cold-saturated aqueous solution of oxalic acid. The precipitate was filtered off and repeatedly washed with deionized water and ethanol, then dried and calcined at 1000°C for 2 hours. The resulting oxalate precursor was then homogeneously mixed with a 3% excess of SiO_2 (Evonik, Aerosil 300) in an agate mortar and the mixture was calcined at 1200°C for 5 hours under ambient atmosphere then milled and annealed for 5 hours at 1500°C under a reducing CO atmosphere. The sintered product was manually ground in an agate mortar before it was stirred in deionized water for 30 minutes, filtered and dried at 80°C for several hours.

CL measurements.—The phosphors were mounted by applying a compact layer onto a conductive aluminum tape. All four phosphors were mounted on a single holder together with a (conductive) zinc oxide phosphor. The current onto the ZnO:Zn phosphor was measured. Since the settings of the electron gun were not changed for the UV-phosphors, the current hitting these phosphors did not change either after moving the sample holder to one of the UV-phosphor positions. Fig. 1 is a sketch of the vacuum system with sample and spectrometer arrangements.

The CL measurements were carried out in a high vacuum chamber at a vacuum level of about 1×10^{-6} mbar using a Kimball Physics Inc., USA electron gun (EFG-7) and power supply (EGPS-7). CL measurements were taken over a range of electron beam accelerating voltages from 5 to 15 kV; deflection plates enabled optimum positioning of the electron beam on the samples.

The CL spectra at a resolution of 0.5 nm were recorded with a Bentham M300 monochromator (UK) between 210 and 650 nm. This spectrometer was equipped with a 2400 grooves/mm grating blazed at 250 nm and slits of 0.37 mm. The spectrometer was calibrated with a deuterium lamp using a CL3 irradiance standard. The window between the quartz fiber bundle and the vacuum was sapphire. The other window (two glass plates) was used to monitor the radiance of ZnO:Zn in the visible part of the spectrum. This radiance was measured with a Jeti Radiometer (Spectrobos 1200, Germany) between 380 and 780 nm.

The conductive phosphor ZnO:Zn does not charge under electron bombardment. This allows accurate current measurements to be made, after suppressing secondary electron emission by biasing the ZnO:Zn at +20 V.[15,16] Unlike current measurements using a Faraday cup, this approach does not include the backscattered electrons, which are not suppressed by the low voltage biasing. Primary electrons that are backscattered, however, deposit very little energy into the sample. Given that backscattering yields are a function of morphology, composition and beam energy, this approach has the additional advantage of better reproducibility. The current density was adjusted to 1.4 μA/cm^2 for the ZnO:Zn reference and the UV-phosphors. This current density is below the saturation limit of the investigated phosphors.

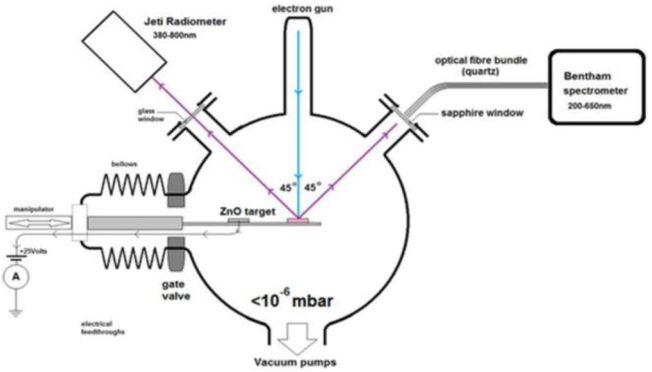

Figure 1. Measuring system of CL. The sample holder also contains ZnO:Zn powder which is used as a reference. CL is measured using a Jeti Radiometer in the visible part of the spectrum, the high resolution Bentham spectrometer is used to collect UV and visible radiation via a sapphire window. The sample holder can be moved horizontally.

Photoluminescence spectroscopy. (VUV).—The VUV spectrometer used herein consists of an Edinburgh Instruments FL920 spectrofluorimeter, which is equipped with a VUV excitation arm instead of the common UV/Vis excitation arrangement. The whole excitation unit is completely integrated into the FL920 spectrofluorimeter system. This VUV excitation arm consists of a D_2 discharge lamp (DS-775), an Acton Research VM-504 VUV-monochromator as well as a mirror-based focusing unit. The monochromator is equipped with manually controlled micrometer-screw entrance and exit slits, as well as a 1200 grooves per millimeter (g/mm) and a 2400 g/mm grating. The VUV monochromator and the whole focusing unit are evacuated by a directly flanged turbo drag pump to realize a pressure of about 3.4×10^{-5} mbar. The D_2 lamp directly irradiates into the optical path of the evacuated monochromator through an MgF_2 window. The remaining distance between the focusing unit, capped with another MgF_2 window, and the sample, which is placed in the non-evacuated FLS920 sample chamber is constantly flooded with a dry stream of N_2 to ensure VUV/UV exposure of the sample material. Sample emission is measured in a fixed 90° arrangement. The detection branch, which is constantly kept at −20°C by Peltier cooling, consists of a convex quartz collection lens, a Czerny-Turner Optics TMS300 monochromator equipped with a 1800 g/mm grating and a photomultiplier tube (PMT, Hamamatsu R928) running in single photon counting mode. All measurements were conducted on thoroughly powdered samples, which were placed in circular sample holders crafted from Spectralon. A correction file for the emission spectra was obtained from a D_2 lamp (range: 200–320 nm) as well as a tungsten incandescent lamp (range: 320–800 nm) certified by NPL (National Physics Laboratory, UK). Emission spectra were recorded at 160 nm excitation using the 1200 g/mm grating excitation, the 1800 g/mm emission grating, excitation slit widths of 2nm and emission slit widths of 1 nm.

Scanning electron microscopy (SEM).—SEM images were taken on a Zeiss EVO MA10 scanning electron microscope, equipped with a LaB_6 cathode. The images were detected by the mounted SE-detector applying an acceleration voltage of 10 kV and a probe current of 1 pA under high vacuum condition at around $5 \cdot 10^{-7}$ mbar. Powder

Table I. PSD data of the as-synthesized UV-C emitting phosphors.

Sample	$Y_2SiO_5:Pr^{3+}$	$YPO_4:Pr^{3+}$	$YBO_3:Pr^{3+}$	$YPO_4:Bi^{3+}$
d_{10} [μm]	3.2	3.7	1.6	1.4
d_{50} [μm]	5.7	6.6	3.2	5.6
d_{90} [μm]	9.7	11.1	5.6	14.8

samples were deposited onto sample holders which were previously equipped with adhesive, conductive (carbon-loaded) pads and directly measured without prior sputtering or other pre-treatment.

Powder X-ray diffraction (PXRD).—Phase formation and purity was investigated by using a Rigaku MiniFlex II diffractometer, working in Bragg–Brentano (Φ/2Φ) geometry and being equipped with a copper anode (Cu-K_α = 0.145 nm). Diffraction data was collected within a 2Φ range from 10° to 80° with a step width of 0.02°.

Particle size determination (PSD).—Measurements of the particle size distributions were conducted on a Horiba LA-950 device. The powdered samples were dispersed in deionized water and then measured for the particle size distribution by dynamic light scattering after exposure to ultrasound for 10 minutes.

Results and Discussion

All samples XRD patterns are shown in Fig. 2 these were of single phase, i.e. showed an XRD pattern in agreement with published reference patterns (PCD entries).[17–19]

In order to evaluate whether the four different phosphor types had comparable particle size and morphology, the PSD was determined and SEM images of all samples were taken. Table I lists the d_{10}, d_{50} and d_{90} values of all four samples demonstrating that all materials are μ-scale powders with an average particle size in the 3–7 μm range.

The SEM images shown in Fig. 3 demonstrated that the YPO_4:Bi and YPO_4:Pr samples have a very similar particle morphology, which is obviously due to the presence of the same host lattice material. In contrast, YBO_3:Pr and Y_2SiO_5:Pr show somewhat smaller primary particles, which are also more spherical. This is probably a result of the sinter active starting materials SiO_2 and H_3BO_3 (the latter decomposes to B_2O_3).

In the Figs. 4–7 show the CL spectra of $YPO_4:Pr^{3+}$, $Y_2SiO_5:Pr^{3+}$, $YBO_3:Pr^{3+}$ and $YPO_4:Bi^{3+}$, respectively recorded at 15 keV and 1.4 μA/cm^2. The spectra between 400 and 650 nm are presented at a different scale and refer to a current density of 1 μA/cm^2. The spectral radiance in these figures is represented in an arbitrary unit, but the values may be compared with each other.

The spectra of the three Pr^{3+} activated phosphors presented in Figs. 4 to 6 all show significant UV-C emission. $YPO_4:Pr^{3+}$ has a set of four emission bands between 225 nm and 280 nm, $Y_2SiO_5:Pr^{3+}$ has two broad emission bands between 250 nm and 350 nm and $YBO_3:Pr^{3+}$ has a group of four emission bands between 250 nm and 325 nm. There is a report[4] of the photoluminescent (PL) spectra of both $YPO_4:Pr^{3+}$ and $YBO_3:Pr^{3+}$ in which the emission bands are at the same positions and have a similar appearance to those that appear in Figs. 4a and 6a, the authors assign these emission bands to broad-band $[Xe]4f^15d^1 \rightarrow [Xe]4f^2$ ($^3H_{6,5,4}$,$^3F_2$) inter-configurational transitions of Pr^{3+}. It is assumed that the two broad emission bands between 250 and 350 nm of $Y_2SiO_5:Pr^{3+}$ (Figure 5a) can also be ascribed to other 4f5d inter-configurational transitions.

It is worth noting that the Pr^{3+} UV-C emission band pattern can be shifted between 220 and 320 nm by the choice of the host matrix, i.e. by the crystal-field splitting and by the centroid shift.[5] This is outlined by Fig. 8 (bottom), since the lower edge of the lowest crystal-field component of the $[Xe]4f^15d^1$ configuration shifts to lower energy from YPO_4 to Y_2SiO_5. However, the efficiency of the phosphor (see below) will also be host matrix dependent.

The broad emission band centered at 375 nm in the spectrum of $YPO_4:Pr^{3+}$ in Figure 4b, which we assign to a $^1S_0 \rightarrow {}^1D_2$ transition, is only just apparent in the photoluminescent spectrum presentedin Ref. 4, and was not previously assigned.

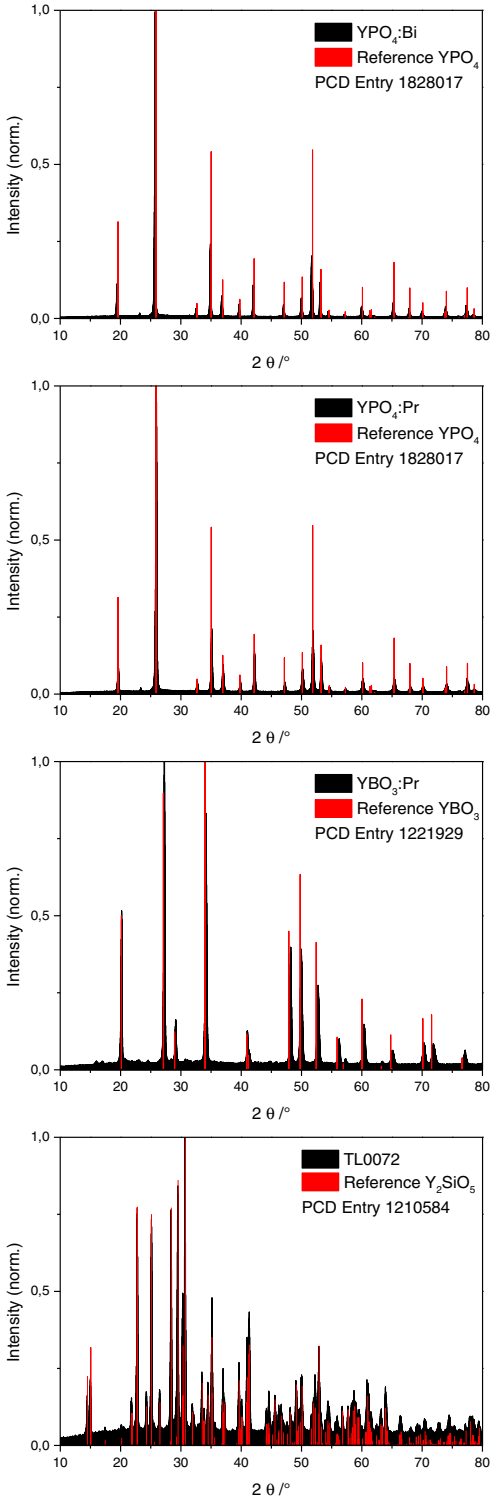

Figure 2. PXRDs of the as-synthesized samples compared to the reference patterns.[17–19]

The emission bands (Figures 4b and 6b) centered around 450 nm in both $YPO_4:Pr^{3+}$ and $YBO_3:Pr^{3+}$ [4] were assigned to $[Xe]4f^15d^1 \rightarrow [Xe]4f^2$ (^3P_J, $^1I_6$) and we assign the broad set of emission bands in $Y_2SiO_5:Pr^{3+}$ around 500 nm (Figure 5b) to the same transition.

The narrow emission band centered at 489 nm in $YPO_4:Pr^{3+}$ was assigned to the $^3P_0 \rightarrow {}^3H_4$ transition[4] which may originate from the

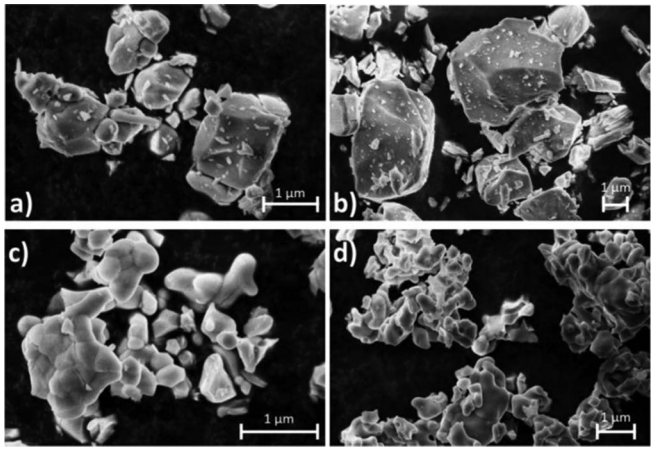

Figure 3. SEM images of typical YPO_4:Bi (a), YPO_4:Pr (b), YBO_3:Pr (c), and Y_2SiO_5:Pr (d) powders, in each case a 1 µm bar is shown.

lowest 4*f*5d state. However they show this band as a single band, whereas clearly we have evidence for it being made up of two very narrow emission bands (see Fig. 4b). Similarly we can distinguish two sharp small bands in same region in the spectrum of YBO_3:Pr^{3+} (Fig. 6b) which we also assign to the $^3P_0 \rightarrow {}^3H_4$ transition. These bands were just barely visible in the photoluminescent spectrum.[20]

The photoluminescent emission spectrum of YPO_4:Pr^{3+} in the range 470 nm to 650 nm has been presented by others,[22] however the

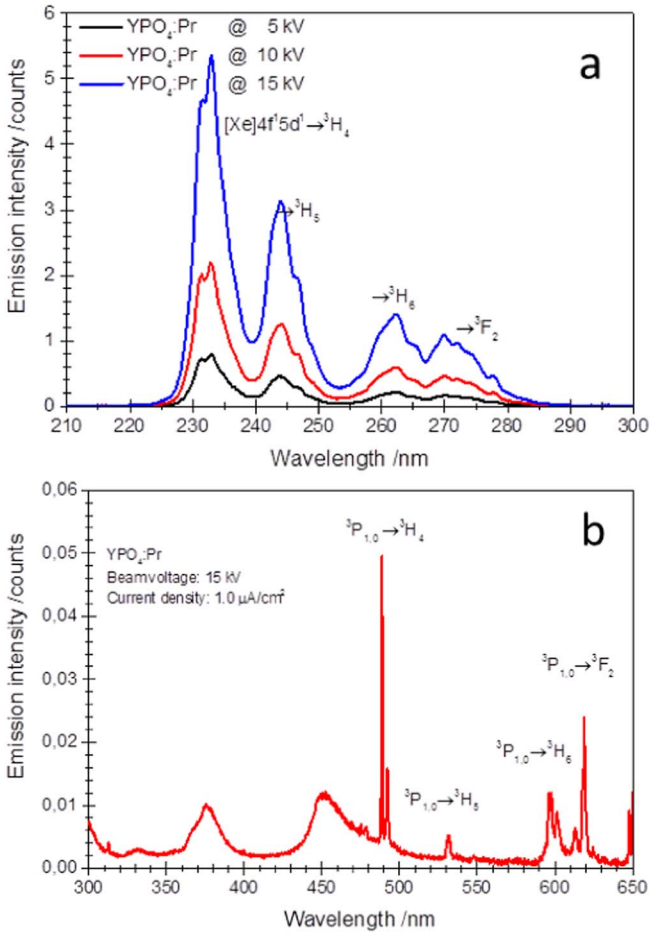

Figure 4. CL spectrum of YPO_4:Pr^{3+}. (a) between 220 nm and 300 nm at 1.4 µA/cm^2. (b) between 300 and 650 nm at 1.0 µA/cm^2, (in b the ordinate has been magnified 100 times).

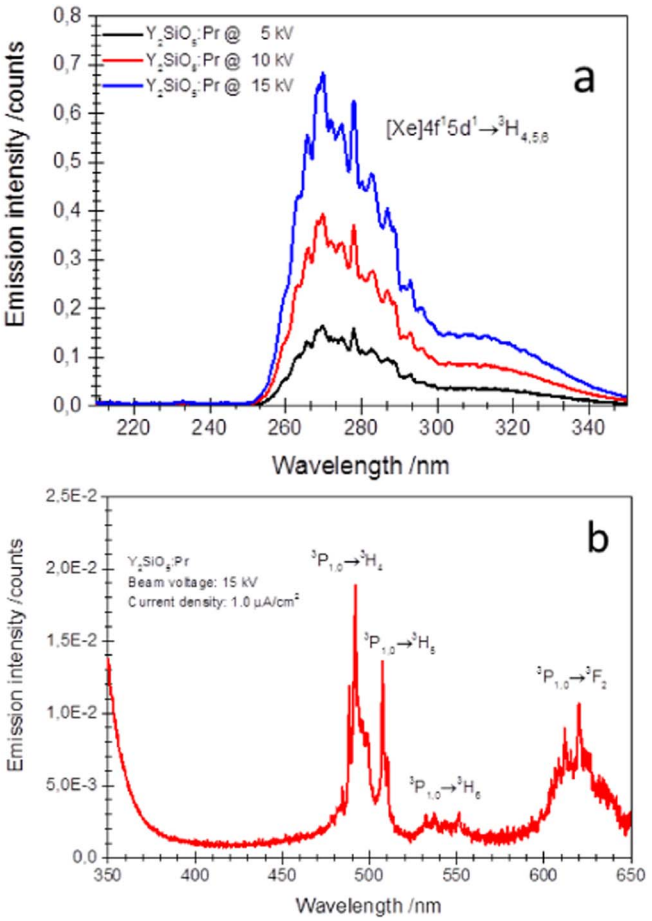

Figure 5. CL spectrum of Y_2SiO_5:Pr^{3+}. (a) between 210 nm and 350 nm at 1.4 µA/cm^2. (b) between 350 and 650 nm at 1.0 µA/cm^2, (in b the ordinate has been magnified 32 times).

resolution of our cathodoluminescent spectrum presented in Figure 4b is better. The previous work[22] suffered from a rising background at the high energy end due to being excited by 450 nm light. However, we agree with the emission band assignments presented previously;[6] these emission bands shown in Figure 4b are at 550 nm (due to $^3P_0 \rightarrow {}^3H_5$), between 590 nm and 618 nm (due to $^1D_2 \rightarrow {}^3H_4$) and the very sharp band at 620 nm (in the red due to $^3P_0 \rightarrow {}^3H_6$) the final emission band seen rising at 650 nm (is due to the $^3P_0 \rightarrow {}^3F_2$ transition).

The CL spectra of the phosphors illustrated in Figures 4–7 and the PL spectra illustrated in Figure 8 show interesting differences. For example, the ratio of the emission peaks of YPO_4:Pr^{3+} at 235 nm and 245 nm is different for the PL and the CL spectra. Also the ratio of the emission peaks of YPO_4:Pr^{3+} and Y_2SiO_5:Pr^{3+} in the UV at 235 nm and in the visible at 490 nm is different for the PL and CL spectra. In the case of the latter difference we assume that the population density of the Pr^{3+} levels $^3P_1$ and $^3P_0$ for CL excitation is lower than in the case of UV-excitation at 160 nm. We plan to investigate these spectral differences in a forthcoming study.

Finally, the energy efficiency upon CL excitation was determined. The energy efficiency η of CL is defined as the ratio of the power density P_r of the CL and the power density P_e of the E-beam that hits the phosphor layer (expressed in %):

$$\eta = \frac{100 P_r}{P_e} \quad [1]$$

The power density of the E-beam is the product of beam voltage and current density at the sample. This requires accurate determination of the area of the sample, while the measurement of the current requires a correction for the secondary electron emission. This was achieved

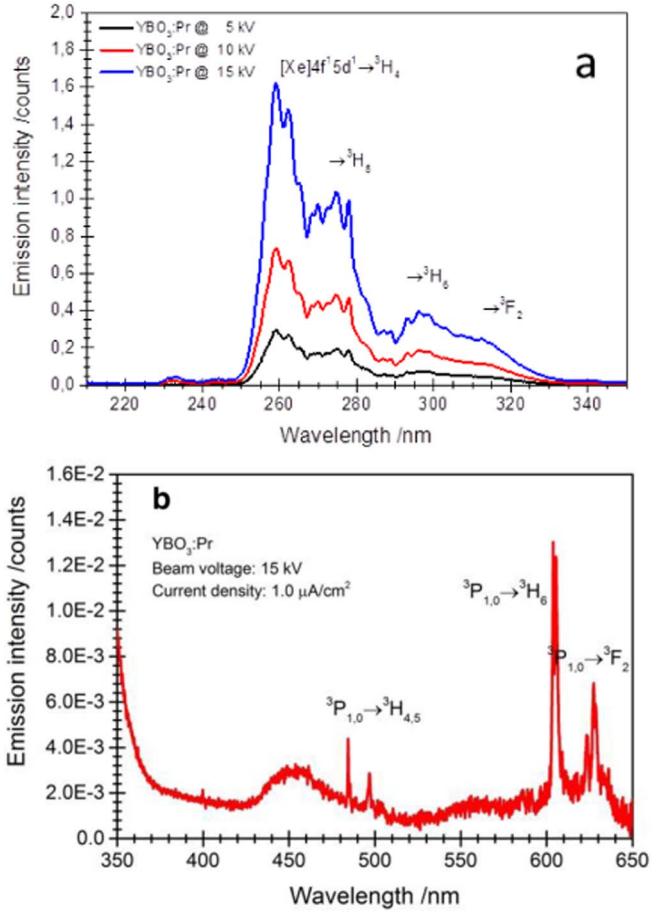

Figure 6. CL spectrum of $YBO_3:Pr^{3+}$. (a) between 210 nm and 350 nm at 1.4 μA/cm^2. (b) between 350 and 650 nm at 1.0 μA/cm^2, (in b the ordinate has been magnified 125 times).

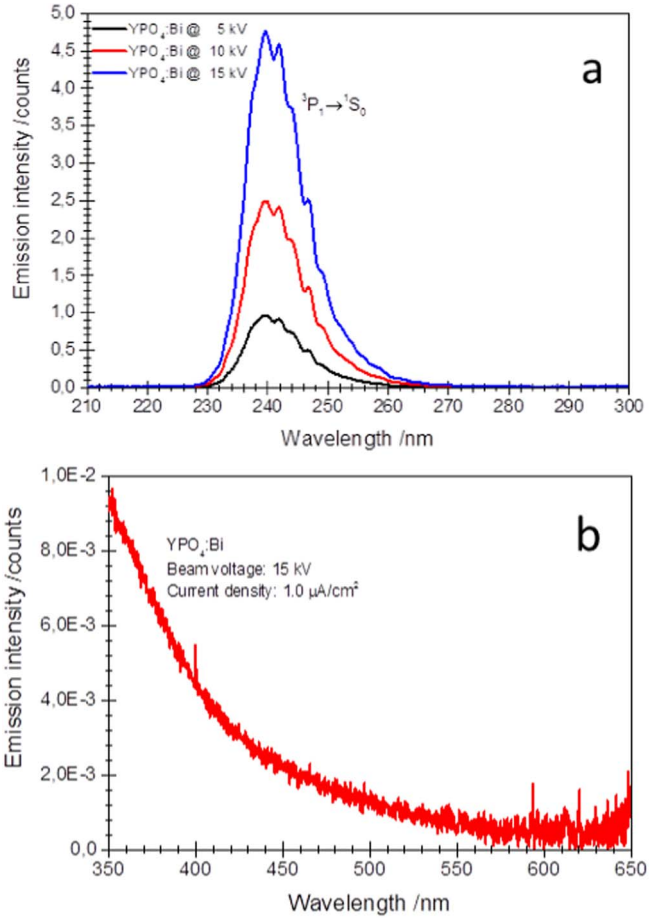

Figure 7. CL spectrum of $YPO_4:Bi^{3+}$. (a) between 210 nm and 300 nm at 1.4 μA/cm^2. (b) between 350 and 650 nm at 1.0 μA/cm^2, (in b the ordinate has been magnified 500 times).

by biasing the sample at + 20 V. At 15 keV and 1.4 μA/cm^2 P_e was 0.021 W/cm^2.

For powder samples the angular distribution of the emitted radiance is assumed to be Lambertian, which means that the power density of the CL can be calculated according to

$$P_r = \pi R \quad [2]$$

where R is the radiance expressed in W/(sr.cm^2). The radiance of the emitted light is defined as:

$$R = \int_a^b SR(\lambda)d\lambda \quad [3]$$

where SR(λ) is the spectral radiance expressed in W/(sr.cm^2. nm) and a and b are the integration limits. However, the spectral radiance is usually measured in arbitrary units, which implies that a calibration procedure is needed to convert the arbitrary values into W/(sr.cm^2. nm). We have recently described a new way for determining the energy efficiency of powder layers of phosphors, in which ZnO was used as a reference to determine the "real" current that hits the phosphor.[15,16] Besides $YPO_4:Pr^{3+}$, $Y_2SiO_5:Pr^{3+}$, $YBO_3:Pr^{3+}$ and $YPO_4:Bi^{3+}$, we have measured the spectral radiance of ZnO in the same way and same settings of the spectrometers, viz. the Bentham and the Specbos. The latter instrument measured the radiance in W/(sr.m^2). We found for η of ZnO at 15 keV 5.4%, which is 23% lower than we found earlier.[16] The reason for this difference is that we have now measured the radiance only in the reflection mode. Therefore herein we take $\eta_{ZnO} = 5.4\%$ as the reference for the UV-phosphors at 15 keV.

Another characteristic of the CL measurement is the transmission through the windows. We used a sapphire window for recording the spectra between 210 and 650 nm. The refractive index of sapphire in the UV region is 1.84 (at 260 nm), which implies that the transmission of UV-radiation through the window is only 83%. In other words, the measured spectral radiances have to be multiplied by a factor of 1.2 for efficiency calculations. The transmission loss through the glass window as shown in Fig. 1 for calculating the efficiency of the ZnO:Zn phosphor has been taken into account. The result of the efficiency calculation is presented in Table II.

In this Table Integral(au) refers to the numerical integration of the UV range of the spectra in arbitrary units, P_r(au) is the Integral corrected for transmission loss in the window and integration over a hemisphere (factor of π in Eq. 2), P_r (in W/cm^2) is the radiated power after multiplication with the calibration factor ($6.83 \cdot 10^{-6}$). The last row contains the energy efficiency for the various phosphors.

In applying the calibration factor obtained from the measured value of 5.4% for ZnO (in the visible part of the spectrum) we have used an essential feature of the Bentham spectrometer: i.e. accurately representing the power distribution of a light source between 220 and 650 nm.

The above presented results confirm that $YPO_4:Bi$, which shows CL and PL spectra solely consisting of a single band due to a $^3P_1$ -$^1S_0$ ([Xe]4f^{14}5d^{10}6s^{1}6p^1 – 6s^2) inter-configurational transition, is a reasonable choice for UV-C emitting fluorescent radiation sources. Moreover, it shows very little thermal quenching up to 300°C[10] and has almost 70% overlap with the germicidal action curve. It also has the second best CL efficiency amongst the four investigated materials.

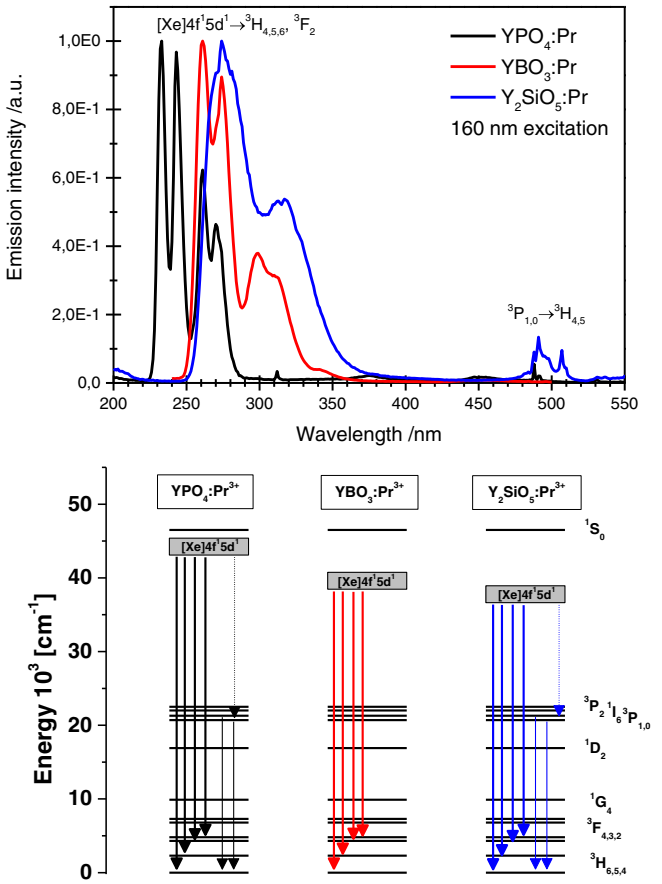

Figure 8. PL spectra of $YPO_4:Pr^{3+}$, $YBO_3:Pr^{3+}$, and ß-$Y_2SiO_5:Pr^{3+}$ (top) upon 160 nm excitation, and a simplified energy level diagram of Pr^{3+} (bottom).

Table II. Energy efficiency of UV emitting phosphors upon 15 keV excitation at 1.4 μA/cm² beam current.

	$Y_2SiO_5:Pr^{3+}$	$YPO_4:Pr^{3+}$	$YBO_3:Pr^{3+}$	$YPO_4:Bi^{3+}$
Band gap [eV]	7.4[24]	9.2[25]	7.5[26]	9.2[25]
Integral [au]	21.9	74.9	41.7	58.8
P, [au]	82.6	282.4	157.2	221.7
P, [W/cm²]	0.00056	0.00193	0.00107	0.00151
η [%]	2.7	9.2	5.1	7.2

A closer look at the three Pr^{3+} activated materials shows that YPO_4:Pr, which was firstly published as an inorganic scintillator,[23] is the most efficient CL phosphor. It also exhibits 80% overlap with the germicidal action curve, which is clearly higher than the value for YBO_3:Pr (70%) and Y_2SiO_5:Pr (60%). Therefore, YPO_4:Pr is the most efficient and effective phosphor for UV-C radiation sources using cathode-rays as the primary energy source.

Conclusions

The CL spectra of the UV emitting phosphors $YPO_4:Pr^{3+}$, $Y_2SiO_5:Pr^{3+}$, $YBO_3:Pr^{3+}$, and $YPO_4:Bi^{3+}$ have been recorded and herein we have shown that they are almost identical to the already published photoluminescence spectra. In addition we have determined their CL efficiencies; the most efficient material is YPO_4:Pr ($\eta = 9.2\%$). In view of the latter phosphors large overlap (80%) with the germicidal action curve, this result is encouraging in relation to the development of UV-C emitting CL lamps. Further improvement of these CL phosphors will include the optimization of the particle surface to limit losses in particular upon low electron energy excitation and thus lower electron penetration depths. In addition to this, the optimization of the concentration of the activator species appears to be of great importance to avoid concentration quenching, in which an excited activator passes on its energy to another activator cation in its close vicinity until a local lattice imperfection, which may act as an energy sink, is reached.[27] Furthermore, since the activator efficiency of Bi^{3+} and Pr^{3+} is usually rather high, as proven by earlier photoluminescence investigations, the energy transfer from the host to the activator could be an another opportunity for improvement. An adequate example for this is e.g. given by garnet scintillator materials in which the incorporation of Gd onto the Lu^{3+} or Y^{3+} site, leads to a significant gain of the light yield through an effective energy transfer from the lattice to the activator species via Gd^{3+}.[28]

Acknowledgments

We are grateful to the German ministry for research and education (BMBF) and to the Foundation of the German economy for generous financial support. We are also grateful to the EPSRC and Technology Strategy Board (TSB) for funding the PURPOSE (TP11/MFE/6/1/AA129F; EP-SRC TS/G000271/1) and CONVERTED (JeS no. TS/1003053/1), PRISM (EP/N508974/1) and FAB3D programs. We are finally grateful to the TSB for funding the CONVERT program.

References

1. C. L. Sun, J. F. Li, C. H. Hu, H. M. Jiang, and Z. K. Jiang, *Eur. Phys. J. D*, **39**, 303 (2006).
2. W. Drozdowski, A. J. Wojtowicz, D. Wisniewski, P. Szupryczynski, S. Janus, J.-L. Lefaucheur, and Z. Gou, *J. Alloys Compd.*, **380**, 146 (2004).
3. A. R. Kulesskii, A. M. Korovkin, A. V. Kruzhalov, L. V. Viktorov, and B. V. Shulgin, *Zh. Prikl. Spektrosk.*, **48**, 650 (1998).
4. B. V. Shulgin, A. R. Kulesskii, A. M. Korovkin, V. L. Petrov, and C. V. Podurovskii, *Opt. Spectrosc.*, **68**, 841 (1990).
5. C. Hu, C. Sun, J. Li, Z. Li, H. Zhang, and Z. Jiang, *Chem. Phys.*, **325**, 563 (2006).
6. R. H. Clapp and R. J. Ginther, *Opt. Soc. Am.*, **37**, 355 (1947).
7. B. Eliasson and U. Kogelschatz, *Appl. Phys. B*, **46**, 299 (1988).
8. R. P. Mildren and R. J. Carman, *J. Phys. D: Appl. Phys.*, **34**, L1 (2001).
9. M. Salvermoser and D. E. Murnick, *Appl. Phys. Lett.*, **83**, 3722 (2003).
10. T. Jüstel, P. Huppertz, W. Mayr, and D. U. Wiechert, *J. Lumin.*, **106**, 225 (2004).
11. T. Jüstel, J. Dirscherl, W. Mayr, and D. U. Wiechert, 6,938,970 US B1 (2002).
12. T. Jüstel, G. Heusler, H. von Busch, and W. Mayr, WO 03/075314 A1 (2003).
13. X. Zeng, H. Park, Y. Kim, S. Jang, S. Son, G. Kim, and S. Lee, US 2006/0001353 (2006).
14. L. Ozawa, *Cathodoluminescence - Theory and Applications*, p. 53, VCH, Cambridge (1990).
15. D. den Engelsen, P. Harris, T. G. Ireland, R. Withnall, and J. Silver, *ECS J. Solid State Sci. Technol.*, **2**, R201 (2013).
16. D. den Engelsen, P. Harris, T. G. Ireland, and J. Silver, *ECS J. Solid State Sci. Technol.*, **3**, R53 (2014).
17. R. Lcomba-Perales, D. Errandonea, Y. Meng, and M. Bettinelli, *Phys. Rev. B: Condens. Matter Mater. Phys.*, **81**, 064113 (2010).
18. S. Hosokawa, Y. Tanaka, S. Iwamoto, and M. Inoue, *J. Mater. Sci.*, **43**, 2276 (2008).
19. C. Cannas, A. Musinu, G. Piccaluga, and S. Enzo, *J. Solid State Chem.*, **178**, 1526 (2005).
20. F. T. You, S. H. Huang, C. X. Meng, D. W. Wang, J. H. Xu, Y. Huang, and G. B. Zhang, *J. Lumin.*, **122–123**, 58 (2007).
21. T. Jüstel, *Recent Developments on UV Emitting Phosphors*, 8th Phosphor Global Summit San Diego, CA, March 25th, 2010.
22. A. Lecointre, A. Bessiere, A. J. J. Bos, P. Dorenbos, B. Viana, and S. Jacquart, *J. Phys. Chem.*, **115**, 4217 (2011).
23. R. C. Naik, N. P. Kranjikar, and N. A. Narasimham, *Solid State Comm.*, **38**, 389 (1981).
24. E. Coetsee, J. J. Terblans, O. M. Ntwaeaborwa, and H. C. Swart, *Phys. B*, **404**, 4426 (2009).
25. A. J. J. Bos, P. Dorenbos, A. Bessière, and B. Viana, *Rad. Meas.*, **43**, 222 (2008).
26. T. Watrous-Kelley and A. L. Diaz, *Chem. Mater.*, **18**, 3130 (2006).
27. D. L. Dexter and J. H. Schulman, *J. Chem. Phys.*, **22**, 1063 (1954).
28. N. Cherepy, S. A. Payne, S. Asztalos, and W. W. Moses, *IEEE Transactions Nuclear Science*, **56**, 873 (2009)